Changes in Terrestrial Water Storage in the Three-North region of China over 2003-2021: Assessing the Roles of Climate and Vegetation restoration

Ajiao Chen[1], Jinghua Xiong[1], Shixue Wu[2,3], Yuting Yang[1,*]

1 State Key Laboratory of Hydroscience and Engineering, Department of Hydraulic Engineering, Tsinghua University, Beijing, China

2 Institute of Urban and Industrial Water Management, Technische Universität Dresden, Dresden, Germany

3 Department Hydrogeology, Helmholtz Centre for Environmental Research – UFZ, Leipzig, Germany

*Corresponding author: Yuting Yang (Yuting_Yang@tsinghua.edu.cn)

Abstract

Large-scale vegetation restoration has markedly enhanced ecosystem services in the Three-North (TN) region, concurrently exacerbating the pre-existing water resource crisis stemming from climate change in this arid domain. However, the specific contributions of climate and vegetation changes to the evolution of water resources in the TN region have yet to be elucidated. This study leverages data from the Gravity Recovery and Climate Experiment (GRACE) and its Follow-on mission (GRACE-FO), specifically the terrestrial water storage anomaly (TWSA) from 2003 to 2021. We identify two TWSA rising (*TWSA_rI* and *TWSA_rII*) and two declining (*TWSA_dI* and *TWSA_dII*) hotspots in the TN region. By exploring the relative importance of climate drivers and vegetation dynamics in influencing the temporal dynamics of TWSA, we found that vegetation restoration assumes a more pivotal role than climate factors in 45.2% of the total area within the identified hotspots, predominantly evident in TWSA declining hotspots. The heightened TWSA in *TWSA_rI* and *TWSA_rII* primarily stems from precipitation recharge, with precipitation-dominated areas constituting 19.3% of the area within the identified hotspots. Potential evapotranspiration dominates TWSA changes in only 4.6% of the region within the identified hotspots, primarily scattered in *TWSA_dI* and *TWSA_dII*. Furthermore, a comparative assessment of soil moisture and groundwater responses to environmental factors indicates that water storage at shallower layers is more responsive to climate factors, while the impacts of vegetation changes on TWSA are more discernibly reflected in water storage at deeper layers. These findings furnish scientific guidance for future ecological restoration planning and sustainable water resources management.

Keywords: Vegetation restoration, Terrestrial water storage, Three-North region of China, GRACE

1 Introduction

The dynamic shifts in climate conditions, marked by increased precipitation variability and elevated temperatures, exert profound effects on both global and regional hydrological cycles (Schewe et al., 2014; Chang et al., 2020; Patterson et al., 2022). Besides climate change, anthropogenic activities contribute significantly to the modification of hydrological cycles too, encompassing alterations to land cover, exploitation of water resources, and the implementation of ecological restoration projects, among other factors (Wada et al., 2017; Huang et al., 2023). Globally, hydrological systems in arid regions generally exhibit heightened sensitivity to external environmental influences in contrast to their humid counterparts (Molnar, 2001; Xie et al., 2015). The Three-North (TN) region in China, encompassing its northern, northeastern, and northwestern sectors, stands as a substantial arid expanse grappling with a dual challenge: a water resource crisis induced by climate change and additional water resource depletion resulting from large-scale vegetation restoration initiatives (Jia et al., 2017; Lv et al., 2019; Liu et al., 2023a; Zhou et al., 2023). These challenges impede the sustainable development and utilization of regional water resources in the TN region.

Vegetation restoration endeavors typically manifest in heightened evapotranspiration rates and reduced runoff volumes, potentially influencing precipitation patterns by reinforcing local moisture recycling (Bai et al., 2020; Zhang et al., 2022; Yang et al., 2023). Given the diverse impact of these alterations in individual hydrological flux on the land water budget, changes in terrestrial water storage emerge as an intuitive indicator for assessing the overarching influence of vegetation restoration on total water resources (Zhao et al., 2021). Terrestrial Water Storage Anomalies (TWSA) data derived from the Gravity Recovery and Climate Experiment (GRACE) satellites indicate recent TWSA depletion attributed to vegetation restoration in various revegetation areas in China, such as the Mu Us Sandyland (Zhao et al., 2021), the Yellow River Basin (Cao et al., 2022), and the Loess Plateau (Liu et al., 2023a).

Terrestrial water storage changes represent a complex interplay of influences

stemming from both climate change and human activities. Numerous studies have endeavored to discern the relative contributions of distinct factors shaping TWSA dynamics in prominent basins across China. For instance, Li et al. (2020) identified increased vegetation as the primary driver behind the decline in TWSA within the Yellow River basin. In the northeastern basins, Li et al. (2023) elucidated a more substantial impact of vegetation on TWSA trends, contrasting with basins in southern China where precipitation emerged as the predominant factor. However, the specific delineation of the relative contributions of climatic factors and vegetation restoration to TWSA changes within the TN region remains unexplored.

Furthermore, soil moisture and groundwater, integral components of terrestrial water storage, have frequently served as pivotal metrics for evaluating shifts in regional water resources prompted by vegetation restoration initiatives. For instance, Jia et al. (2017) observed a diminution in soil moisture associated with afforestation, while Gao et al. (2015) documented notable declines in groundwater levels resulting from large-scale revegetation endeavors. In contrast, Han et al. (2020) reported an increase in soil moisture in the Loess Plateau of China, and Ellison et al. (2017) posited that reforestation could enhance infiltration capacity and groundwater recharge. These disparities underscore the necessity of comprehensive investigations into the responses of soil moisture and groundwater to the combined influences of climate change and vegetation restoration. Such insights are imperative for a nuanced understanding of water resource dynamics in the TN region, where knowledge in this domain remains limited.

As a result, the primary objectives of the current study are (1) to systematically characterize the temporal evolution of TWSA in the TN region of China over the preceding two decades (2003–2021); (2) to attribute the observed TWSA changes to pertinent climate-related variables and the impacts of artificial revegetation; and (3) to discern and systematically compare the nuanced responses of soil moisture and groundwater to variations in environmental factors. The precise identification and attribution of alterations in terrestrial water storage, coupled with a thorough

examination of soil moisture and groundwater dynamics within areas subjected to revegetation initiatives, are essential for the comprehensive evaluation of ecological restoration endeavors. Furthermore, the insights derived from this study carry substantial implications for guiding future planning initiatives in the realm of sustainable water resource management.

2 Materials and methods

2.1 Study region

The TN region, encompassing 4 million square kilometers and constituting 42% of China's land area, spans across 13 provinces, autonomous regions, and municipalities as illustrated in Fig. 1. Characterized as a typical arid and semi-arid expanse, a majority of its regions receive an average annual precipitation of less than 400 mm. The TN region predominantly features bare and grassland, with relatively low forest coverage, rendering it susceptible to land degradation, desertification, and dust storms. In response to these challenges, the Chinese government initiated an extensive vegetation restoration effort since 1978 in the TN region, with plans for continuation until 2050.

Over the past few decades, a noteworthy surge in vegetation coverage has been observed in the TN region, particularly evident in the forest coverage rate, which escalated from 5.05% in 1978 to 13.57% in 2018 (State Forestry and Grassland Administration, 2018). These initiatives have yielded significant ecological benefits for the region, including soil stabilization, a reduction in dust storm occurrences, and climate regulation. However, they have introduced a paradoxical challenge by exacerbating water scarcity within the region. These features make the TN region stands as an ideal research area for detecting and attributing changes in terrestrial water storage induced by both climate-related factors and vegetation restoration.

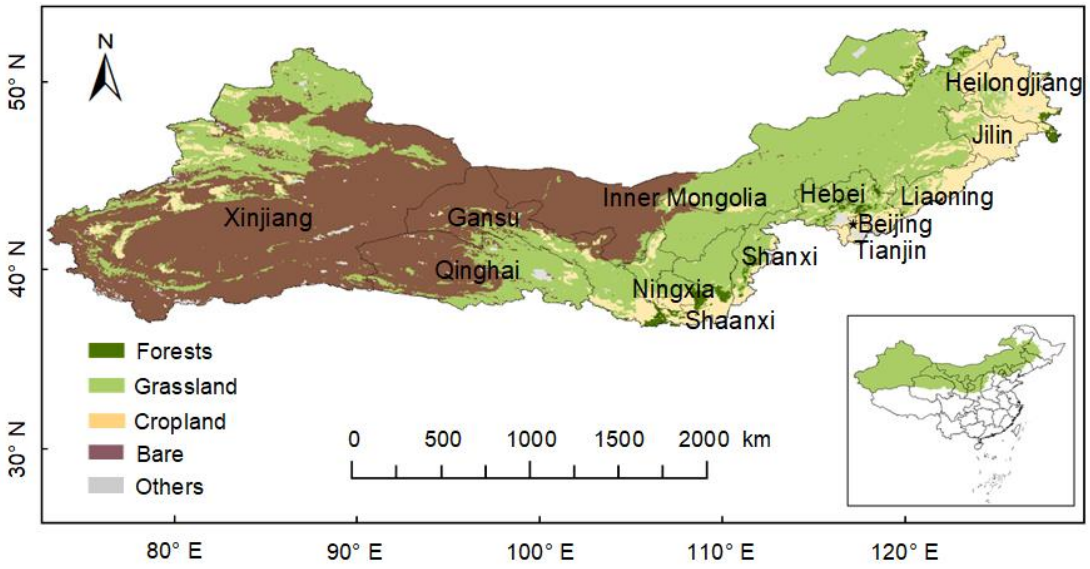

Figure 1. Geographical delineation of the study area.

2.2 Datasets

2.2.1 Water storage

Monthly TWSA datasets employed in this study were derived from both the GRACE and its successor, the GRACE Follow-on (GRACE-FO) satellites. We utilized GRACE/GRACE-FO mascon solutions from three institutions: Jet Propulsion Laboratory (JPL) (http://grace.jpl.nasa.gov) (Landerer and Swenson, 2012), Center for Space Research (CSR) (http://www2.csr.utexas.edu/grace) (Save et al., 2016), and Goddard Space Flight Center (GSFC) (https://earth.gsfc.nasa.gov/geo/data/grace-mascons) (Loomis et al., 2019). The JPL mascon product was employed with specified gain factors, which were obtained from http://grace.jpl.nasa.gov. These mascon series utilize regularization techniques in data processing, enabling the direct computation of variations in terrestrial water storage from Level 1B data (Save et al., 2016). This approach eliminates the need for filtering, smoothing, and other empirical scaling techniques, thereby reducing errors and providing enhanced signal-to-noise ratios and spatial resolutions (Watkins et al., 2015; Save et al., 2016). An overlapping period of JPL, CSR, and GSFC TWSA datasets from 2003 to 2021 was chosen as our study period. An ensemble mean of these datasets was adopted to mitigate uncertainties associated with data processing. CSR TWSA data, initially provided at a

spatial resolution of 0.25° × 0.25°, were resampled to 0.5° × 0.5° to maintain consistency with the resolutions of JPL and GSFC TWSA data. Linear interpolation of adjacent months or averaging monthly TWSA values from adjacent years for a specific month was applied to address missing values (Andrew et al., 2017; Chen et al., 2019).

To gain further insights into changes in TWSA, soil moisture (0–1 m, including the surface layer and the root zone) and groundwater data were obtained from Global Land Data Assimilation System Catchment Land Surface Model (GLDAS_CLSM) outputs. The model is driven by meteorological datasets from the European Center for Medium-Range Weather Forecasts (ECMWF) (Li et al., 2019). Groundwater calculation involves subtracting the sum of canopy water, snow water equivalent, and soil moisture from total water storage. The GLDAS_CLSM_2.2 provides daily-scale soil moisture and groundwater data at a spatial resolution of 0.25° × 0.25° (https://disc.gsfc.nasa.gov/datasets/GLDAS_CLSM025_DA1_D_2.2/summary?keywords=GLDAS), which were converted into monthly time series at a resolution of 0.5° × 0.5° for this study to facilitate analysis.

2.2.2 Meteorological variables

Monthly precipitation (*P*) data were sourced from the Multi-Source Weighted-Ensemble Precipitation (MSWEP, https://www.gloh2o.org/mswep/) dataset (Beck et al., 2019). This dataset, offering an optimal ensemble of gauge observations, satellite retrievals, and climate reanalysis, provides precipitation information at a spatial resolution of 0.1° × 0.1°. Monthly potential evapotranspiration (PET) was obtained from the Global Land Evaporation Amsterdam Model (GLEAM v3.7b, https://www.gleam.eu/) at a spatial resolution of 0.25° × 0.25° (Miralles et al., 2011; Martens et al., 2017), where PET is estimated from the Priestley-Taylor model. Both *P* and PET data were resampled to a spatial resolution of 0.5° × 0.5° to be consistent with the TWSA data.

2.2.3 Vegetation index

Vegetation changes were evaluated using the Normalized Difference Vegetation Index (NDVI). Monthly NDVI data obtained from the Moderate Resolution Imaging Spectroradiometer (MODIS, https://neo.gsfc.nasa.gov/view.php?datasetId=MOD_NDVI_M) were employed in this study (Didan et al., 2015). These data were acquired at a spatial resolution of 0.5° × 0.5° and were derived from MODIS/Terra Vegetation Indices L3 Global 0.05 Deg CMG V006 (MOD13C1 and MOD13C2).

2.3 Attribution analyses

To attribute the temporal changes of monthly TWSA, we first employed a stepwise multiple linear regression (Draper and Smith, 1998; Clow, 2010) to identify significant predictor variables, assessed at a 5% significance level through an F-test, explaining the temporal variability of TWSA for each grid cell. Subsequently, we applied the dominance analysis approach (Azen and Budescu, 2003) to assess the relative importance of the identified variables. In contrast to conventional methods providing an overall evaluation of variable importance, dominance analysis explores the unique contribution of each predictor by considering all possible subsets of variables. This method entails constructing multiple regression models for each subset and quantifying the extent to which each predictor dominates in explaining the variance of the dependent variable. The dominance weight, computed as the difference in the average coefficient of determination (R^2) between models including and excluding a particular predictor, serves to quantify the relative importance of each variable. This approach accommodates interactions and collinearity among predictors, providing a nuanced understanding of their individual contributions (Vize et al., 2019). The resulting dominance weights facilitate the ranking of predictors based on their average relative importance, contributing to a relatively comprehensive interpretation of variable significance within the entire model context.

3 Results

3.1 Hotspots of TWSA changes in the TN region

The linear trend of TWSA was assessed for each grid cell in the TN region spanning

from 2003 to 2021, utilizing TWSA datasets provided by JPL, CSR, and GSFC. Hotspots exhibiting consistent and significant increasing or decreasing trends across the three datasets were identified (Supplementary Fig. S1), resulting in the delineation of two TWSA rising (*TWSA_rI* and *TWSA_rII*) and two TWSA declining (*TWSA_dI* and *TWSA_dII*) regions (Fig. 2). Specifically, *TWSA_rI*, predominantly located in the northeastern part of the study area (primarily within Heilongjiang province), covered 7.0% of the total grid cells within the identified hotspots. *TWSA_rII*, situated in the southwestern part (mainly within Qinghai province), encompassed 19.6% of the total grid cells within the four hotspots. *TWSA_dI*, spanning portions of Beijing, Tianjin, and the provinces of Hebei, Shanxi, Liaoning, Shaanxi, as well as the Inner Mongolia and Ningxia Hui Autonomous regions, exhibited the largest coverage (43.4%) among the identified hotspots. *TWSA_dII* (geographically associated with the Xinjiang Uygur Autonomous Region) represented 30.0% of the total grid cells within the four hotspots. The areal average TWSA (ensemble mean of JPL, CSR, and GSFC TWSA datasets) over these hotspots is also presented in Fig. 2. Both TWSA rising (declining) hotspots displayed significant increasing (decreasing) trends, with all trends being statistically significant at the 0.05 significance level.

Spatial trends in GLDAS-derived soil moisture anomalies (SMA) and groundwater anomalies (GWSA) in the identified hotspots are illustrated in Figs. 3a and b, respectively. Generally, both SMA and GWSA demonstrated increasing trends in *TWSA_rI* and *TWSA_rII* and decreasing trends in *TWSA_dI* and *TWSA_dII* from 2003 to 2021. However, the trends of SMA were generally weaker than those of GWSA, attributable to the GLDAS_CLSM's definition of soil moisture as the water storage in the top 1 meter of the soil, containing a comparatively smaller amount of water compared to groundwater (Supplementary Fig. S2). In addition, the areal average time series of SMA and GWSA in the four hotspots of TWSA changes are illustrated in Figs. 3c–f. Similar to TWSA, both SMA and GWSA exhibited significant increasing trends in *TWSA_rI* and *TWSA_rII*, with corresponding significant decreasing trends in *TWSA_dI* and *TWSA_dII*. Notably, the amplitudes of groundwater were larger than

those of soil moisture in the identified hotspots.

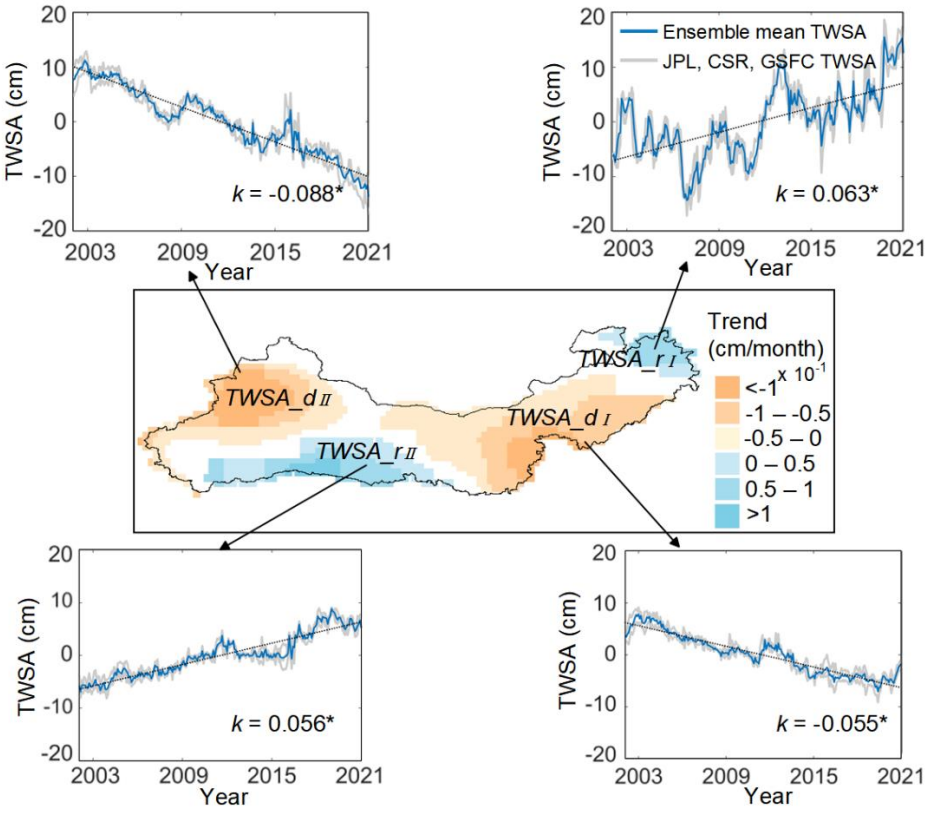

Figure 2. Spatial distribution of TWSA hotspots exhibiting significant rising trends (*TWSA_rI* and *TWSA_rII*) and declining trends (*TWSA_dI* and *TWSA_dII*), alongside the interannual variations in areal average TWSA (ensemble mean derived from JPL, CSR, and GSFC TWSA datasets) during the period 2003–2021 within the specified hotspots. The symbol "*" denotes instances where the linear trend (*k*) is statistically significant at the 5% significance level.

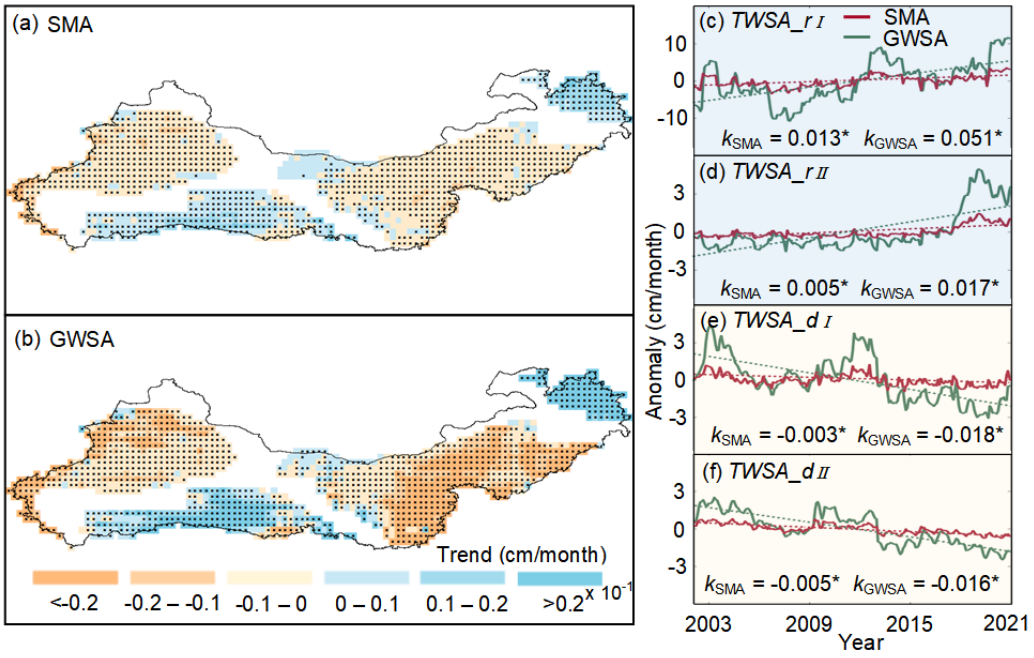

Figure 3. Spatial trend maps depicting (a) soil moisture anomalies (SMA) and (b) groundwater anomalies (GWSA) in the four identified hotspots during the period 2003–2021. Interannual variations of SMA and GWSA are presented for (c) *TWSA_rI*, (d) *TWSA_rII*, (e) *TWSA_dI*, and (f) *TWSA_dII*. The symbol "*" denotes instances where the linear trend (*k*) is statistically significant at the 5% significance level.

3.2 Attribution of TWSA changes

In this study, the atmospheric water supply (*P*) and demand (PET) are regarded as crucial climate drivers influencing TWSA, and their impacts are compared with those of artificial vegetation restoration, as indicated by changes in the NDVI. The linear trends of these three environmental factors (*P*, PET, and NDVI) across the four identified hotspots are presented in Fig. 4. Precipitation has exhibited an increase in 81.0% of the total grid cells within the four hotspots, with 46.3% of them being statistically significant at the 0.05 significance level (Fig. 4a). Grid cells displaying decreasing precipitation were observed in *TWSA_rII*, *TWSA_dI*, and *TWSA_dII*, although none of these trends passed the significance test (Fig. 4b). PET showed a decreasing trend in 50.4% of the total grid cells within the four hotspots, and the significantly decreasing PET (29.9%) was predominantly observed in *TWSA_rII*, *TWSA_dII*, and the western part of *TWSA_dI* (Figs. 4c–d). Conversely, PET displayed

an increasing trend in 49.6% of the grid cells within the four hotspots, with 46.9% of them passing the significance test. Significant increases in PET were mainly observed in the Loess Plateau region of China, situated in *TWSA_dI* (Fig. 4c). Additionally, NDVI exhibited an increasing trend in 92.6% of the grid cells within the four hotspots, with 83.0% of them being statistically significant, indicating a notable greening of vegetation in the TN region over the past two decades (Figs. 4e–f). The most conspicuous greening area was identified in the Loess Plateau region, where the Grain to Green Program (GTGP), recognized as the largest ecological restoration plan ever in a developing country (Wang et al., 2016), has been implemented since 1999.

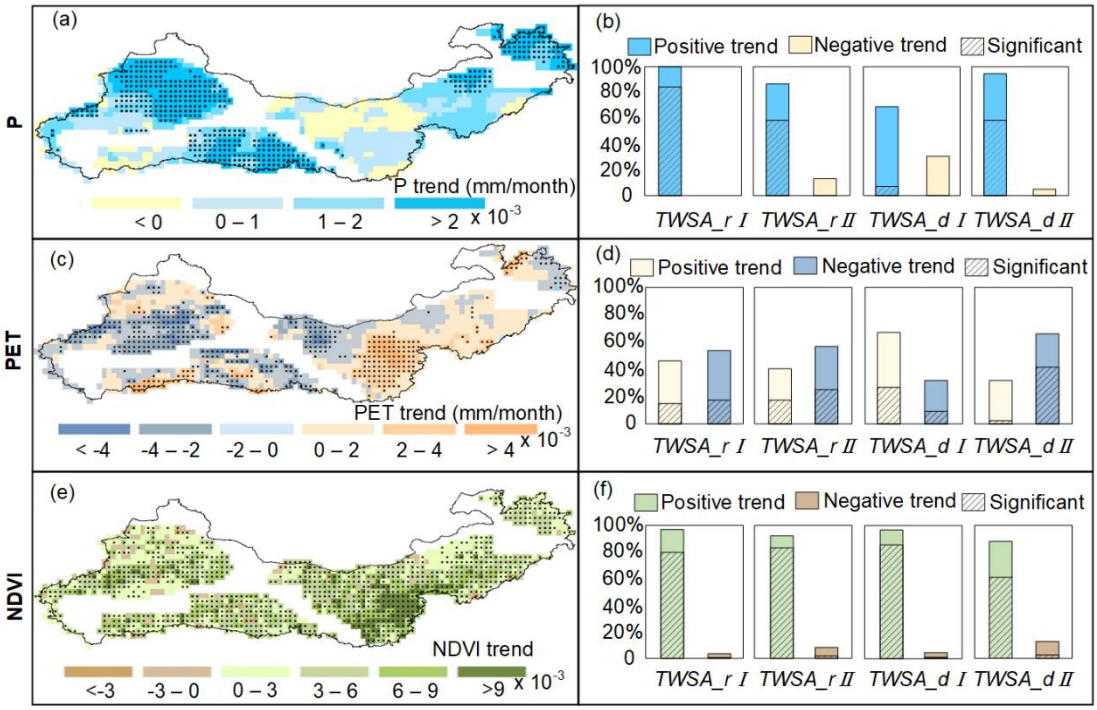

Figure 4. Spatial distribution and histograms illustrating the trends of (a–b) precipitation (*P*), (c–d) potential evapotranspiration (PET), and (e–f) vegetation index (NDVI) across the four identified hotspots during the period 2003–2021.

Figures 5a–c respectively present the relative importance, as indicated by the R^2 values derived from the dominance analysis, of *P*, PET, and NDVI in elucidating the temporal variability of monthly TWSA in the four identified hotspots. 70% of the grid cells within the identified hotspots were selectively displayed based on the criterion that the total explanatory power of the three influencing factors (*P*, PET, and NDVI)

surpassed the 5% significance level, represented by graded colors. TWSA changes in gray areas were not significantly associated with either the two climate-related factors or vegetation restoration during the study period from 2003 to 2021. In general, *P* played a more pivotal role than PET and NDVI in influencing TWSA changes in *TWSA_rI* and *TWSA_rII* (Fig. 5d–e). Conversely, NDVI exhibited greater relative importance than climate-related factors in explaining the temporal variability of TWSA in *TWSA_dI* and *TWSA_dII* (Figs. 5 f–g).

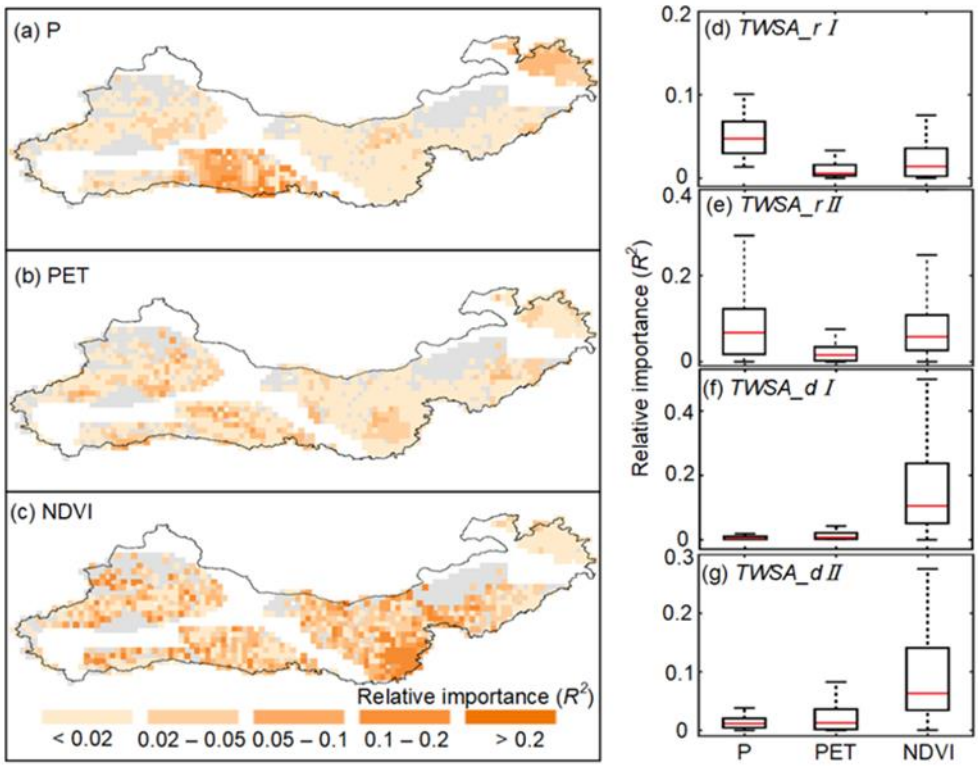

Figure 5. Spatial distribution of the relative importance (R^2) of (a) *P*, (b) PET and (c) NDVI in explaining TWSA temporal variability (areas in gray means none of the environmental factor has been selected as significant predictor variable in explaining TWSA temporal variability). The comparisons of the relative importance of each environmental factor in the four hotspots: (d) *TWSA_rI*, (e) *TWSA_rII*, (f) *TWSA_dI* and (g) *TWSA_dII*.

Subsequently, the dominant driver influencing TWSA was identified through comparing the relative importance of *P*, PET, and NDVI at each grid cell. As illustrated in Fig. 6a, nearly half of the area (45.2%) within the four identified

hotspots exhibited TWSA changes primarily dominated by NDVI. Areas dominated by *P* and PET accounted for 19.3% and 4.6% of the grid cells within the hotspots, respectively. Specifically, *P*-dominant areas were predominantly situated in regions where TWSA exhibited significant increasing trends (i.e., *TWSA_rI* and *TWSA_rII*). Conversely, in regions with TWSA displaying significant decreasing trends (i.e., *TWSA_dI* and *TWSA_dII*), NDVI predominantly drove the observed TWSA changes. While the NDVI in *TWSA_dII* generally exhibited a weaker increasing trend compared to that in *TWSA_dI*, it's important to note the relatively shallow groundwater table in *TWSA_dII* (Fan and Miguez-Macho, 2013), where vegetation heavily relies on groundwater. Consequently, even a modest increase in NDVI within *TWSA_d II* could potentially result in a decline in TWSA. These outcomes underscore the replenishing effects of precipitation on terrestrial water storage and the impact of vegetation restoration in consuming terrestrial water storage.

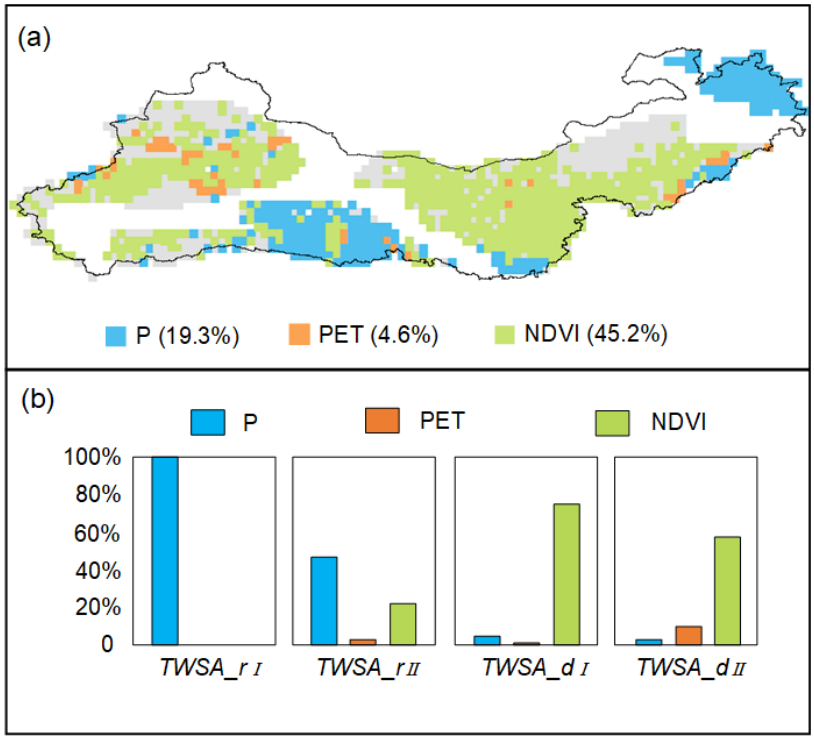

Figure 6. (a) Spatial distribution and (b) histograms illustrating the dominant influencing factor among *P*, PET and NDVI for TWSA temporal variability in the four identified hotspots.

3.3 Comparison of SMA and GWSA responses to environmental changes

As water storage at different layers of the soil may respond differently to environmental changes, we additionally conducted a comparative analysis of the relative importance of *P*, PET, and NDVI in elucidating the temporal variability of SMA and GWSA in the four identified hotspots, as depicted in Fig. 7. Climate-related factors, specifically *P* and PET, generally exhibited a larger relative importance in explaining the temporal variability of SMA than in elucidating changes in GWSA across the identified hotspots. Additionally, NDVI demonstrated a more pronounced relative importance in elucidating changes in GWSA compared to its role in explaining SMA in all identified hotspots. This observation suggests that water storage in shallower layers is more susceptible to influences from climate-related factors, while deeper layers exhibit a higher degree of responsiveness to dynamics in vegetation.

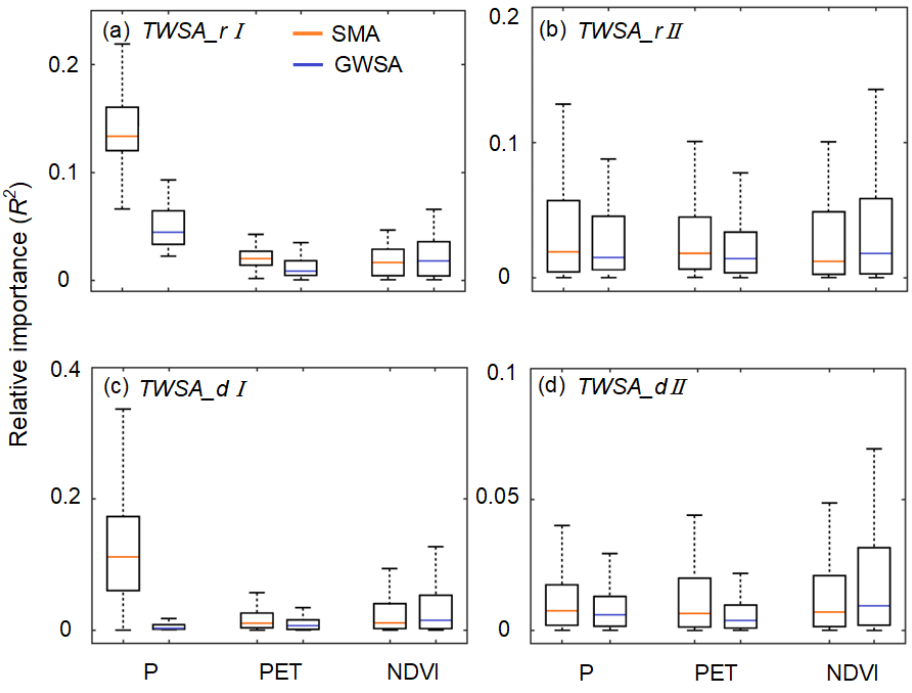

Figure 7. Relative importance of *P*, PET and NDVI in explaining SMA and GWSA temporal variability in (a) *TWSA_rI*, (b) *TWSA_rII*, (c) *TWSA_dI* and (d) *TWSA_dII*.

By comparing the relative importance of *P*, PET and NDVI in explaining SMA and GWSA, dominant influencing factors for SMA and GWSA changes were identified in Fig. 8. The temporal variability of SMA and GWSA was primarily governed by

precipitation in 37.9% and 11.5% of the grid cells within the four identified hotspots, as illustrated in Figs. 8a and c. In regions characterized by increased SMA and GWSA (i.e., *TWSA_rI* and *TWSA_rII*), climate-related factors exerted a more substantial influence than NDVI on water storage across larger areas. Notably, increased precipitation emerged as the predominant driver, replenishing water storage at both shallow and deep layers.

In regions displaying decreased SMA and GWSA (i.e., *TWSA_dI* and *TWSA_dII*), water storage at the shallow layer exhibited greater responsiveness to climate-related factors (e.g., decreased precipitation and increased PET), leading to a decline in SMA in approximately 50% of grid cells in *TWSA_dI* and *TWSA_dII* (Fig. 8b). Concurrently, water storage depletion at the deep layer was predominantly driven by increased NDVI, with NDVI dominating TWSA changes in over 50% of the areas in *TWSA_dI* and *TWSA_dII* (Fig. 8d).

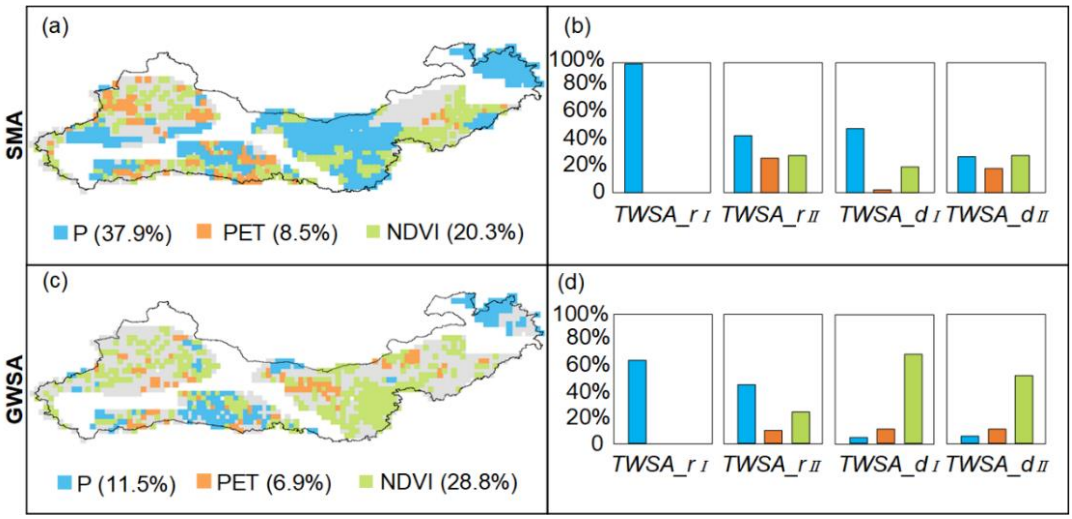

Figure 8. Spatial distribution and histograms illustrating the dominant influencing factor among *P*, PET and NDVI for (a–b) SMA and (c–d) GWSA temporal variability in the four identified hotspots.

4 Discussion

In the context of climate change and vegetation restoration, a comprehensive understanding of the evolutionary dynamics and underlying causes of TWSA in arid regions is imperative. Here we identified a noteworthy reduction in TWSA across

nearly three-quarters of the TN region, encompassing extensive areas of the Loess Plateau (identified as *TWSA_dI*) and northwestern China (identified as *TWSA_dII*). Attribution analysis indicates that the primary factor contributing to the declining TWSA in these regions is enhanced water consumption induced by vegetation restoration. This observation suggests a potential over-planting phenomenon in these areas, which is also supported by earlier studies (e.g., Liu et al., 2023a; Liu et al., 2023b). Conversely, we also identified two TWSA rising hotspots within the TN region, specifically *TWSA_rI* in the northeastern sector and *TWSA_rII* in the southwestern region, which was primarily due to precipitation replenishment that surpassed the water consumption associated with vegetation restoration. Additionally, increased TWSA in *TWSA_rII* may be partially ascribed to glacial mass gain in the Karakoram Mountains (Karakoram anomaly) (Forsythe et al., 2017; Farinotti et al., 2020) and the expansion of lakes in the Tibetan Plateau's endorheic basin (Zhang et al., 2017; Li et al., 2022). These findings highlight the intricate dynamics of the impact of vegetation restoration on TWSA, emphasizing that its influence is not universally associated with a decline in TWSA. Precipitation replenishment emerges as a crucial factor capable of substantially or entirely offsetting the augmented water consumption resulting from vegetation restoration. Therefore, the continuation of revegetation initiatives is deemed suitable in regions where the positive effects of precipitation recharge outweigh the negative impact of additional water consumption by extra vegetation. This recommendation aligns with the guidance provided by Xu et al. (2023), who propose a similar strategy for semiarid and subhumid areas in northern China. In these regions, where the benefits stemming from climate change surpass the adverse contributions of vegetation to soil moisture, the ongoing efforts in revegetation are advised. Conversely, in hyperarid and arid subareas, a focus on nature-based recovery is recommended.

In addition to examining total water storage changes, this study addresses the knowledge gap regarding water storage variations at different soil depths in the TN region. The results reveal a noteworthy consistency in trends between SMA and

GWSA, with GWSA exhibiting a larger magnitude. The reduced GWSA observed in *TWSA_dI* and *TWSA_dII* aligns with findings from previous studies. Specifically, Han et al. (2020) documented GWSA depletion in the Loess Plateau of China (corresponding to *TWSA_dI*) during 2003–2015, while Liu et al. (2023b) reported a decline in GWSA in northwestern China (associated with *TWSA_dII*) from 2003 to 2018. The decline in SMA within *TWSA_dI* and *TWSA_dII* also aligns with earlier studies by Jia et al. (2017) and Liu et al. (2023b), respectively. However, it is noteworthy that Han et al. (2020) reported an increased SMA in specific areas within the Loess Plateau, attributing it to the positive impact of the water conservancy system in Ningxia and Hetao irrigation areas. This disparity underscores the complexity of accurately detecting changes in water storage, emphasizing the necessity of considering the influence of various anthropogenic activities.

Notably, anthropogenic mass flow signals in GRACE/GRACE-FO observations attributed to coal mining and transportation (Tang et al., 2013; Zhou et al., 2023), as well as domestic and industrial water consumption and irrigation (Felfelani et al., 2017), were not specifically accounted for. The stronger decreasing trends in GRACE-derived TWSA compared to GLDAS model-derived TWSA in both *TWSA_dI* and *TWSA_dII* (Supplementary Fig. S3) suggest potential influences from the aforementioned human activities. Annual water consumption records from the National Bureau of Statistics (http://www.stats.gov.cn/sj/ndsj/) for *TWSA_dI* and *TWSA_dII* reveal a notable rise in domestic, industrial, agricultural, and ecological water consumption over the past two decades (Supplementary Figs. S4a and b). These regions, corresponding to areas of groundwater over-exploitation in China (Huang et al., 2023), align with the North China Plain for *TWSA_dI* and the Tarim Basin for *TWSA_dII*. In addition, a decline in TWSA and GWSA was observed during the period 2003–2009 (Figs. 2 and 3c), which might also be related to the increased water consumption due to human activities (Fig. S4c). Thus, it is evident that, in addition to artificial vegetation restoration, water consumption resulting from diverse human activities has also contributed to TWSA depletion.

In addition, the causal relationship between vegetation and TWSA revealed herein should be viewed with caution. We assume that the observed increase in vegetation over the TN region can largely be attributed to human-led ecological restoration projects, but it should be noted that the survival and subsequent growth of artificially planted vegetation were heavily contingent upon local water conditions (McVicar et al., 2007). Our results showed that increased TWSA in around 20.0% area of *TWSA_rII* was dominated by NDVI (Fig. 6). This might be explained by the enhanced water retention capacity of soil that benefits from increased vegetation. More extensive vegetation coverage and improved root systems could facilitate water infiltration and soil hydrophilicity (Lange et al., 2009; Guan et al., 2010; Wang et al., 2013; Chen et al., 2021), and consequently impede runoff formation and contribute to increases in terrestrial water storage. This issue deserves further exploration in the future.

5 Conclusions

This study utilized TWSA data derived from the GRACE and GRACE-FO missions to examine water storage dynamics within the context of climate change and vegetation restoration in the TN region from 2003 to 2021. Four distinctive hotspots were identified, characterized by either ascending (*TWSA_rI* and *TWSA_rII*) or descending (*TWSA_dI* and *TWSA_dII*) trends in TWSA. These findings were corroborated by soil moisture and groundwater data obtained from the GLDAS model.

To attribute the observed regional TWSA changes to climatic drivers (*P* and PET) and artificial vegetation restoration, dominance analysis was applied to assess the relative importance of *P*, PET, and NDVI in influencing the temporal variability of TWSA. Results indicated that vegetation exerted a more pronounced influence than climate-related factors on TWSA changes in descending TWSA hotspots (*TWSA_dI* and *TWSA_dII*), while precipitation predominantly governed TWSA changes in most ascending TWSA hotspots (*TWSA_rI* and *TWSA_rII*) during the study period. Regions dominated by NDVI constituted 45.2% of the area within the identified hotspots,

while those dominated by *P* and PET covered 19.3% and 4.6% of the area, respectively. Furthermore, our study revealed that water storage at shallow layers exhibited heightened responsiveness to climate-related factors, whereas the impacts of vegetation changes on TWSA were more discernible in water storage at deeper layers. In summary, the outcomes of this study contribute valuable insights into the evolution and causative factors of TWSA changes in the TN region. Additionally, they offer scientific guidance for sustainable water resource management and inform decision-making processes related to future ecological restoration initiatives.

CRediT authorship contribution statement

Ajiao Chen: Conceptualization, Methodology, Formal analysis, Resources, Writing – original draft, Funding acquisition. Jinghua Xiong: Resources, Writing – review & editing. Shixue Wu: Conceptualization, Methodology. Yuting Yang: Conceptualization, Methodology, Writing – review & editing, Supervision, Funding acquisition.

Declaration of Competing Interest

The authors declare that they have no known competing financial interests or personal relationships that could have appeared to influence the work reported in this paper.

Acknowledgments

This study is financially supported by the National Natural Science Foundation of China (No. 42071029), the Chinese Academy of Sciences (Grant No. xbzg-zdsys-202103) and Postdoctoral Research Foundation of China (2023M731990).

References

Andrew, R., Guan, H., Batelaan, O. (2017). Estimation of GRACE water storage components by temporal decomposition. *Journal of Hydrology*, 552, 341–350.

Azen, R & Budescu, D. (2003). The dominance analysis approach for comparing predictors in multiple regression. *Psychological Methods*, 8 (2), 129–148.

Bai, P., Liu, X., Zhang, Y., Liu, C. (2020). Assessing the impacts of vegetation greenness change on evapotranspiration and water yield in China. *Water Resources Research*, 56 (10), e2019WR027019.

Beck, H., Wood, E., Pan, M., Fisher, C., Miralles, D., van Dijk, A., McVicar, T., and Adler, R. (2019). MSWEP V2 global 3-hourly 0.1° precipitation: methodology and quantitative assessment. *Bulletin of the American Meteorological Society*, 100(3), 473–500.

Cao, Y., Xie, Z., Woodgate, W., Ma, X., Cleverly, J., Pang, Y., Qin, F., Huete, A. (2022). Ecohydrological decoupling of water storage and vegetation attributed to China's large-scale ecological restoration programs. *Journal of Hydrology*, 615, 128651.

Chang, L.., Yuan, R., Gupta, H., Winter, C., Niu, G. (2020). Why is the terrestrial water storage in dryland regions declining? A perspective based on Gravity Recovery and Climate Experiment satellite observations and Noah land surface model with multiparameterization schemes model simulations. *Water Resources Research*, 56, e2020WR027102.

Chen, A., Guan, H., Batelaan, O., Zhang, X., He, X. (2019). Global soil moisture-air temperature coupling based on GRACE-derived terrestrial water storage. *Journal of Geophysical Research: Atmospheres*. 124 (14), 7786–7796.

Chen, A.J., Guan, H.D., Batelaan, O. (2021). Seesaw terrestrial wetting and drying between eastern and western Australia. *Earths Future*, 9 (5), e2020EF001893.

Clow, D. (2010). Changes in the timing of snowmelt and streamflow in Colorado: a response to recent warming. *Journal of Climate*, 23 (9), 2293–2306.

Didan, K., Barreto Munoz, A., Solano, R., Huete, A. (2015). MODIS vegetation index users guide.

Draper, N & Smith, H. (1998). Applied regression analysis. Hoboken, N. J: Wiley Interscience. https://doi.org/10.1002/9781118625590

Ellison, D., Morris, C., Locatelli, B., Sheil, D., Cohen, J., Murdiyarso, D., Gutierrez, V., van Noordwijk, M., Creed, I., Pokorny, J., Gaveau, D., Spracklen, D., Tobella, A.B., Ilstedt, U., Teuling, A., Gebrehiwot, S., Sands, D., Muys, B., Verbist, B., Springgay, E., Sugandi, Y., Sullivan, C. (2017). Trees, forests and water: Cool insights for a hot world. *Global Environmental Change*, 43, 51–61.

Fan, Y & Miguez-Macho, G (2013). Global patterns of groundwater table depth. *Science*, 339 (6122): 940–943.

Farinotti, D., Immerzeel, W., de Kok, R., Quincey, D., Dehecq, A. (2020). Manifestations and mechanisms of the Karakoram glacier anomaly. *Nature Geoscience*, 13, 8–16.

Felfelani, F., Wada, Y., Longuevergne, L., Pokhrel, Y (2017). Natural and human-induced terrestrial water storage change: A global analysis using hydrological models and GRACE. *Journal of Hydrology*, 553, 105–118.

Forsythe, N., Fowler, H., Li, X., Blenkinsop, S., Pritchard, D. (2017). Karakoram temperature and glacial melt driven by regional atmospheric circulation variability. *Nature Climate Change*, 7, 664–670.

Gao, Z., Zhang, L., Cheng, L. (2015). Groundwater storage trends in the Loess Plateau of China estimated from streamflow records. *Journal of Hydrology*, 530, 281–290.

Guan, H., Simunek, J., Newman, B., Wilson, J. (2010). Modelling investigation of water partitioning at a semiarid ponderosa pine hillslope. *Hydrological Processes*, 24, 1095–1105.

Han, Z., Huang, S., Huang, Q., Bai, Q., Zheng, X. (2020). Effects of vegetation restoration on groundwater drought in the Loess Plateau, China. *Journal of Hydrology*, 591, 125566.

Huang, Z., Yuan, X., Sun, S., Leng, G., Tang, Q. (2023). Groundwater depletion rate over China during 1965–2016: The long-term trend and inter-annual variation. *Journal of Geophysical Research: Atmospheres*, 128, e2022JD038109.

Jia, X., Zhu, Y., Luo, Y. (2017). Soil moisture decline due to afforestation across the Loess Plateau, China. *Journal of Hydrology*, 546, 113–122.

Landerer F and Swenson, S. (2012). Accuracy of scaled GRACE terrestrial water storage estimates. *Water Resources Research*, 48, 2011WR011453.

Lange, B., Lüescher, P., Germann, P. (2009). Significance of tree roots for preferential infiltration in stagnic soils. *Hydrology and Earth System Sciences*, 13, 1809–1821.

Li, B., Rodell, M., Kumar, S., Beaudoing, H., Getirana, A., Zaitchik, B. et al. (2019) Global GRACE data assimilation for groundwater and drought monitoring: Advances and challenges. *Water Resources Research*, 55, 7564–7586.

Li, C., Zhang, Y. Q., Shen, Y., Yu, Q. (2020). Decadal water storage decrease driven by vegetation changes in the Yellow River Basin. *Science Bulletin*, 65(22), 1859–1861.

Li, X., Long, D., Scanlon, B, Mann, M., Li, X., Tian, F., Sun, Z., Wang, G. (2022). Climate change threatens terrestrial water storage over the Tibetan Plateau. *Nature Climate Change*, 12, 801–807.

Li, C., Yu, Q., Zhang, Y., Ma, N., Tian, J., Zhang, X. (2023). Dominant drivers for terrestrial water storage changes are different in northern and southern China. *Journal of Geophysical Research: Atmospheres*, 128, e2022JD038074.

Liu, K., Li, X., Wang, S., Zhang, X. (2023a). Unrevealing past and future vegetation restoration on the Loess Plateau and its impact on terrestrial water storage. *Journal of Hydrology*, 617, 129021.

Liu, Q., Xu, Y., Chen, J., Cheng, X. (2023b). Multi-source satellite reveals the heterogeneity in water storage change over northwestern China in recent decades. *Journal of Hydrology*, 624, 129953.

Loomis, B., Luthcke, S., Sabaka, T. (2019). Regularization and error characterization of GRACE mascons. *Journal of Geodesy*, 93, 1381–1398.

Lv, M., Ma, Z., Li, M., Zheng, Z. (2019). Quantitative analysis of terrestrial water storage changes under the Grain for Green program in the Yellow River basin. *Journal of Geophysical Research: Atmospheres*, 124, 1336–1351.

Martens, B., Miralles, D., Lievens, H., van der Schalie, R., de Jeu, R., Fernández-Prieto, D., Beck, H., Dorigo, W., Verhoest, N. (2017). GLEAM v3: satellite-based land evaporation and root-zone soil moisture. *Geoscientific Model Development*, 10, 1903–1925.

McVicar, T., Li, L., Van Niel, G., Zhang, L., Li, R., Yang, Q., Zhang, X., Mu, X., Wen, A., Liu, W., Zhao, Y., Liu, Z., Gao, P (2007). Developing a decision support tool for China's re-vegetation program: Simulating regional impacts of afforestation on average annual streamflow in the Loess Plateau. *Forest Ecology and Management*, 251, 65–81.

Miralles, D., Holmes, T., de Jeu, R.., Gash, J., Meesters, A., Dolman, A. (2011). Global land-surface evaporation estimated from satellite-based observations. *Hydrology and Earth System Sciences*, 15, 453–469.

Molnar, P. (2001). Climate change, flooding in arid environments, and erosion rates. *Geology*, 29 (12), 1071–1074.

Patterson, N., Lane, B., Sandoval-Solis, S., Persad, G., Ortiz-Partida, J. (2022). Projected effects of temperature and precipitation variability change on streamflow patterns using a functional flows approach. *Earth's Future*, 10, e2021EF002631.

Save, H., Bettadpur, S., Tapley, B. (2016). High resolution CSR GRACE RL05 mascons. *Journal of Geophysical Research: Solid Earth*, 121, doi:10.1002/2016JB013007.

Schewe, J., Heinke, J., Gerten, D., Haddeland, I., Arnell, H., Clark, D., Dankers, R., Eisner, S., Fekete, B., Colón-González, F., Gosling, S. (2014). Multimodel assessment of water scarcity under climate change. *Proceedings of the National Academy of Sciences*, 111.9, 3245–3250.

State Forestry and Grassland Administration. 40-Year Comprehensive Evaluation Report of the Three-North Shelterbelt Forest Program; State Forestry and Grassland Administration: Beijing, China, 2018 (in Chinese).

Tang, Q., Zhang, X., Tang, Y. (2013). Anthropogenic impacts on mass change in North China. *Geophysical Research Letters*, 40 (15), 3924–3928.

Vize, C., Collison, K., Crowe, M., Campbell, W., Miller, J., Lynam, D. (2019). Using dominance analysis to decompose narcissism and its relation to aggression and externalising outcomes. *Assessment*, 26, 260–270.

Wada, Y., Bierkens, M., de Roo, A., Dirmeyer, P. , Famiglietti, J, Hanasaki, N., Konar, M., Liu, J., Müller Schmied, H., Oki, T., Pokhrel, Y., Sivapalan, M., Troy, T., van Dijk, A., van Emmerik, T., Van Huijgevoort, M., Van Lanen, H., Vörösmarty, C., Wanders, N., Wheater, H. (2017). Human–water interface in hydrological modelling:

current status and future directions. *Hydrology and Earth System Science*, 21, 4169–4193.

Wang, C., Zhao, C., Xu, Z., Wang, Y., Peng, H. (2013). Effect of vegetation on soil water retention and storage in a semi-arid alpine forest catchment. *Journal of Arid Land*, 5, 207–219.

Wang, S., Fu, B., Piao, S. (2016). Reduced sediment transport in the Yellow River due to anthropogenic changes. *Nature Geoscience*, 9 (1), 38–41.

Watkins, M., Wiese, D., Yuan, D., Boening, C., Landerer, F. (2015). Improved methods for observing Earth's time variable mass distribution with GRACE using spherical cap mascons. *Journal of Geophysical Research: Solid Earth*, 120, 2648–2671.

Xie, X., Liang, S., Yao, Y., Jia, K., Meng, S., Li, J. (2015). Detection and attribution of changes in hydrological cycle over the Three-North region of China: Climate change versus afforestation effect. *Agricultural and Forest Meteorology*, 203, 74–87.

Xu, L., Gao, G., Wang, X., Fu, B. (2023). Distinguishing the effects of climate change and vegetation greening on soil moisture variability along aridity gradient in the drylands of northern China. *Agricultural and Forest Meteorology*, 343, 109786.

Yang, Y., Roderick, M.L., Guo, H., Miralles, D., Zhang, L., Fatichi, S., Luo, X., Zhang, Y., McVicar, T.R., Tu, Z., Keenan, T., Fisher, J., Gan, R., Zhang, X., Piao, S., Zhang, B., Yang, D. (2023). Evapotranspiration on a greening Earth. *Nature Reviews Earth & Environment*, 4, 626-641.

Zhang, G., Yao, T., Shum, C., Yi, S., Yang, K., Xie, H., Feng, W., Bolch, T., Wang, L., Behrangi, A., Zhang, H., Wang, W., Xiang, Y., Yu. J. (2017). Lake volume and groundwater storage variations in Tibetan Plateau's endorheic basin. *Geophysical Research Letters*, 44, 5550–5560.

Zhang, B., Tian, L., Yang, Y., He, X. (2022). Revegetation does not decrease water yield in the Loess Plateau of China. *Geophysical Research Letters*, 49, e2022GL098025.

Zhao, M., Geruo, A., Zhang, J., Velicogna1, I., Liang, C., Li, Z. (2021). Ecological restoration impact on total terrestrial water storage. *Nature Sustainability*, 4(1), 6–62.

Zhou, Y., Dong, J., Cui, Y., et al (2023). Ecological restoration exacerbates the agriculture-induced water crisis in North China Region, *Agricultural and Forest*

610 *Meteorology*, 331, 109341.